Materials and Design 186 (2020) 108311

Contents lists available at ScienceDirect

Materials and Design

journal homepage: www.elsevier.com/locate/matdes

Fracture toughness determination of fused silica by cube corner indentation cracking and pillar splitting

Sebastian Bruns [a,*], Laszlo Petho [b], Christian Minnert [a], Johann Michler [b], Karsten Durst [a]

[a] Physical Metallurgy, TU Darmstadt, Darmstadt, Germany
[b] Empa, Swiss Federal Laboratories for Materials Science and Technology, Thun, Switzerland

HIGHLIGHTS

- The pillar splitting technique is applicable to anomalous behaving glasses.
- Densification plays a minor role in indentation cracking and is negligible for pillar splitting.
- Indentation cracking and pillar splitting deliver similar fracture toughness values.
- Electron beam irradiation affects experiments inside the SEM.

GRAPHICAL ABSTRACT

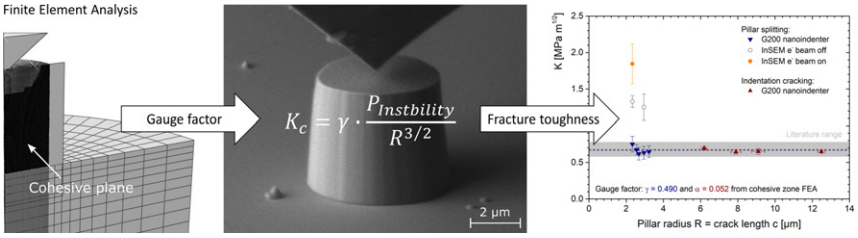

ARTICLE INFO

Article history:
Received 4 September 2019
Received in revised form 24 October 2019
Accepted 25 October 2019
Available online 8 November 2019

Keywords:
Fused silica
Indentation cracking
Pillar splitting
Fracture toughness
Finite element analysis
Electron beam irradiation

ABSTRACT

In this paper the applicability of the pillar splitting technique for fracture toughness determination on anomalous behaving bulk fused silica glass is explored. The results are compared to conventional cube corner indentation cracking analyzed using the Lawn, Evans and Marshall model (JACerS, 63 (1980) 574). The experimental analysis is supported by constitutive Finite Element Analysis with cohesive zones to determine adequate gauge factors to correlate the load instability upon splitting to the fracture toughness Kc. The role of densification on pillar splitting was critically examined.

The results show a fragmentation of the micro pillar into three parts, a failure pattern as proposed by Sebastiani et al. (Philos. Mag., 95 (2014) 1928). Therefore, the applicability of pillar splitting to (anomalous) glasses is confirmed. Cohesive zone FEA delivered the gauge factors required for fracture toughness calculation. The influence of densification on those factors, however, was found to be small for indentation cracking and negligible for pillar splitting. With the corresponding set of gauge factors fracture toughness values in good accordance with literature could be determined. Inside the SEM, moreover, electron beam irradiation has been found to enhance the fracture properties of fused silica.

1. Introduction

In nowadays electronic devices oxide glasses are important structural and functional members. The fracture toughness is a key design parameter for the reliability of glasses in thin film and micro or nano electromechanical applications [1–3]. The determination of fracture toughness on the small length scale has achieved significant advances in the last years [4–6]. New methods like the pillar splitting technique have been developed [4,7] which, however, have never been applied to oxide glasses so far. The mechanic response of glasses is strongly linked to the deformation processes. Normal glasses deform mainly via volume conservative shear flow whereas anomalous glasses as fused silica additionally exhibit the ability to densify their network structure under hydrostatic pressure [8–10]. The influence of densification on indentation cracking is controversially discussed in literature

* Corresponding author.
E-mail address: s.bruns@phm.tu-darmstadt.de (S. Bruns).

https://doi.org/10.1016/j.matdes.2019.108311

[3,11]. However, the densification influence on the pillar splitting technique remains unclear [12].

The indentation cracking behavior of oxide glasses has widely been studied [10,13–15]. It is well known that cone cracking is the predominant crack system active in anomalous glasses as fused silica whereas median/radial cracking with cracks emanating from the corners of the pyramidal indenter dominates in soda lime silica glass, a prototype normal glass. Lawn, Evans and Marshall (LEM) [16] set up a model to quantify indentation fracture toughness relating radial crack length c to indentation load P and the elastic plastic material properties Elastic Modulus E and Hardness H:

$$K_c = \alpha \cdot \left(\frac{E}{H}\right)^{1/2} \cdot \frac{P}{c^{3/2}} \tag{1}$$

Since indentation cracking deals with crack initiation and propagation, a fundamental difference to conventional fracture toughness testing, a factor α is introduced to correlate indentation fracture toughness to the conventional K_c. Lawn et al. [16] already proposed the correlation factor α to depend on the indenters centerline to face angle Ψ. Anstis et al. determined α to 0.016 for Vickers geometry [17]. According to Lee et al. [18] α is proportional to $0.03 \cdot \cot(\Psi)^{3/2}$ which reproduces the value for Vickers geometry remarkably well and delivers a α value of 0.038 for the sharper cube corner tip geometry ($\Psi = 35°$). This is in good agreement with experimentally determined values ranging from 0.032 to 0.054 [19–23]. The wide range of values indicates that α is material dependent and the linearity of α with $\sqrt{E}/H$ is only valid in a small regime and fails when elasticity or plasticity dominate [24]. Also Poisson's ratio was found to influence α [18,25], disproving the general validity of a single α value for a certain indenter geometry.

Equation (1) applies to the median/radial crack system only where the median crack develops during loading followed by a radial crack extension upon unloading when compressive stresses in the vicinity of the contact vanish [11,15]. Simultaneously active other crack systems may be expected to impede the radial crack extension in a way that the K_c estimate is being overestimated using LEM approach [3]. In fused silica, pure radial cracking cannot be realized using Berkovich indenter geometry, since cone cracking is predominant and always present [10]. Switching to sharper indenter geometries such as cube corner triggers radial crack initiation [26]. The cube corner geometry displaces more than three times more material for a given load compared to Berkovich [26]. This reduces the cracking threshold in silica glass by three orders of magnitude from 0.5 to 1.5 N to about 1 mN but increases the likelihood for chipping to occur [19,26–28]. This also applies for other materials and makes the cube corner geometry popular for testing thin film materials and small volumes [23,29,30].

Fracture toughness testing using indentation cracking, however, is influenced by various factors like residual stresses, substrate influences and geometric limitations of thin film materials. The pillar splitting technique developed by Sebastiani and coworkers [4,7] overcomes some of the previous mentioned problems. Pillar Splitting is an advanced indentation cracking technique where the indentation test is performed in the center of a freestanding micro pillar. Pillar preparation is usually performed using focused ion beam (FIB) milling but has also been successfully applied using lithography techniques [31–34]. During indentation testing a median crack is forming inside the pillar and it becomes unstable when reaching the sidewalls. The instability load $P_{Instability}$ can directly be linked to K_c using a parameter γ for correlation:

$$\frac{K_c = \gamma \cdot P_Instability}{R^{3/2}} \tag{2}$$

The parameter γ is usually determined using cohesive zone (CZ) finite element analysis (FEA) [4,7,12]. Thereby γ is determined as a function of the elastic-plastic material properties (E/H). The pillar splitting approach and was recently extended to sharper indenter geometries [12,31] and applied to silicon bulk material [31]. Those studies further question the influence of densification on the γ estimate [12], since γ values present in literature were determined using von Mises plasticity representing volume conservative shear flow only [4,7,12].

In the present paper, the pillar splitting technique is applied to an oxide glasses for the first time. The micro pillar were prepared using the lithography process deep reactive ion etching (DRIE). With this technique a large number of micro pillar can be produced in a single process [32] and a potential damage from FIB milling [31,35] can be avoided. Fused silica is used as model material, thus the question how densification affects the micro pillar cracking behavior is addressed. Pillar splitting experiments are performed under ambient conditions using cube corner geometry as well as inside a scanning electron microscope (SEM). The results are compared to indentation cracking while constitutive cohesive zone FEA is used to study the densification influence on the gauge factors γ and α for pillar splitting and indentation cracking, respectively. Finally those factors are used to calculate fracture toughness values for both approaches.

2. Experimental details

2.1. Lithography based micro pillar fabrication: deep reactive ion etching (DRIE)

A lithography based deep reactive ion etching (DRIE) technique was used to fabricate fused silica micro pillar similar to the study by Ramachandramoorthy and coworkers [32]. A 500 μm thick and 100 mm diameter fused silica wafer was used as a substrate for the microfabrication. The low etch selectivity between the photoresist and silica requires the use of a hard metallic mask. For this purpose, a 500 nm thick aluminum layer was magnetron sputtered onto the front side of the substrate using an Alliance-Concept DP650 deposition system. This layer serves as the mask during plasma etching of the pillars. The back side was coated with 100 nm aluminum in the same machine, as the electrostatic chuck in the plasma etchers require a conductive bottom layer for holding the substrate in place during process.

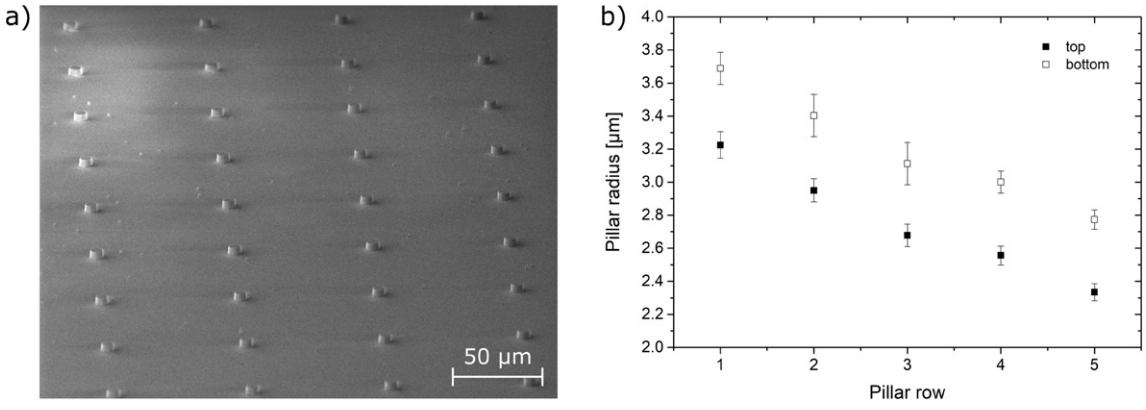

Fig. 1. a) Array of DRIE micro pillars. b) The micro pillar radius was measured in SEM at two positions, at the pillar top and bottom.

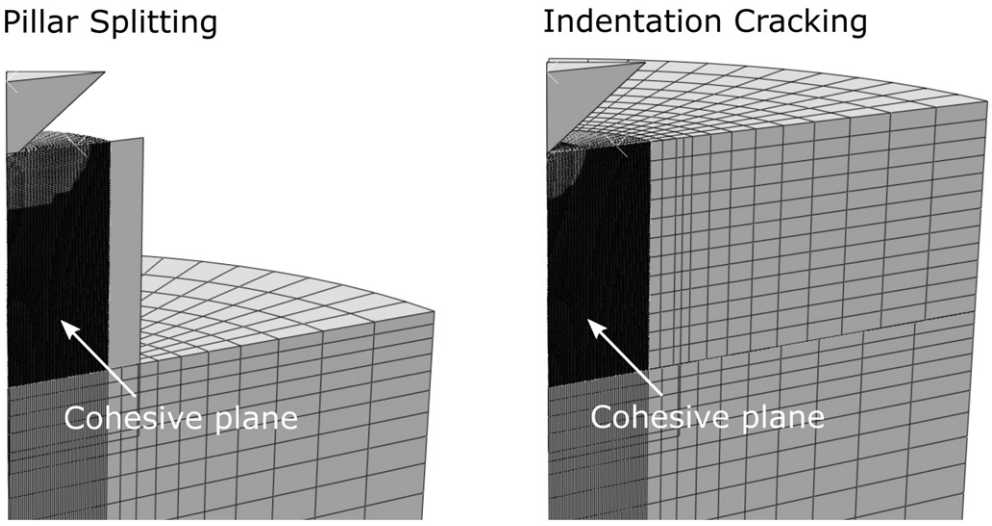

Fig. 2. FEA models for pillar splitting (left) and indentation cracking (right). The cohesive zone is visualized in dark grey with a light grey radial crack propagating along the plane.

To pattern the hard mask, the substrate was spin coated with a 2 μm thick photoresist layer (AZ 1512, Microchemicals GmbH) in a Karl Suss ACS200 automated spincoater, then soft baked at 120 °C for 90 s. A Heidelberg MLA150 direct laser writer patterned the photoresist layer, using a 405 nm laser with 1 μm spot size and a dose of 44 mJ/cm^2. The exposed pattern was cleared by immersion into a developer (MF CD-26, Microchemicals GmbH) in the ACS200 system. The hard mask was patterned in a STS Multiplex ICP plasma etcher system. A mixture of Cl_2 and BCl_3 gases in an RF plasma resulted in a 350 nm/min etch rate. Next, the pattern was transferred into the fused silica substrate in a SPTS APS plasma etcher. A combination of C_4F_8 and O_2 gases removed the silica with a rate of 720 nm/min.

The metallic mask was removed by immersion into a commercial aluminum etchant (ANPE, Microchemicals GmbH), then rinsed in DI water. The wafer was recoated with a 14 μm thick photoresist layer (AZ9260, Microchemicals GmbH), to protect the pillars during the wafer dicing step. A Disco DAD321 automated dicing saw was used to slice the substrate into 10 × 10 mm squares. The protective coating is then removed by rinsing the chip in acetone and isopropanol.

The etching procedure was performed to a depth of roughly 4.2 μm, corresponding to the pillar height. On a single fused silica wafer five different pillar geometries were realized aligned in separated rows with radius increasing in steps of 0.25 μm starting from 2.25 μm. The pillar geometry was measured in SEM at the pillar top and bottom and is visualized in Fig. 1b. A taper angle of roughly 6° can be measured.

2.2. Nanoindentation testing

Nanoindentation testing under ambient conditions was performed using a Keysight G200 nanoindenter. For indentation testing in vacuum a Nanomechanics NanoFlip inside a Tescan Mira3 Scanning Electron Microscope (SEM) was used. Conventional nanoindentation testing was performed with a Berkovich and pillar splitting experiments with a cube corner diamond indenter tip, both produced by Synton-MDP. Tip area function and machine compliance were calibrated before testing on a commercial fused silica reference sample according to the procedure by Oliver and Pharr [36]. Indentation testing was performed in Continuous Stiffness Measurement (CSM) mode with a strain rate $\dot{p}/p$ of 0.05 s^{-1}, where hardness and elastic modulus were averaged over at least 9 tests. Pillar splitting experiments were performed with constant displacement rate of 10 nm/s. Tests inside the SEM are in the following referred to as inSEM, where imaging was performed with an acceleration voltage of 3 kV. The testing axis was aligned 70° to the incident electron beam.

2.3. Finite element analysis

Finite element analysis with cohesive elements was performed using the software package ABAQUS [37]. The indentation cracking process was modelled with a three dimensional 6-fold model exploiting symmetry of a three sided pyramidal indenter tip in a similar manner as in previous studies [4,7,11,18,38]. A 150 μm wide and 300 μm tall micro pillar with a total number of 15000C3D8 elements (aspect ratio 4:1) was constructed on top of a 700 μm wide square substrate block. A plane of square zero-thickness COH3D8 cohesive elements with a size of 1.5 μm was aligned along the indenter edge to model median/radial cracking. For indentation cracking simulations a third block was added next to the micro pillar to extend the model for bulk indentation cracking purpose (Fig. 2).

The contact between cube corner indenter and material surface was assumed to be frictionless. All material properties were presumed to represent rate insensitive room-temperature values with elastic isotropy. An elastic modulus E of 70 GPa and a Poisson's ratio of 0.18 was used for fused silica [11]. The anomalous plastic behavior was modelled using Drucker-Prager-Cap (DPC) plasticity with a yield strength under pure shear $d = 7.5$ GPa and a hydrostatic yield strength $p_b = 8$ GPa. Details on the densification behavior of fused silica and the constitutive model can be found elsewhere [11,40, 41]. The influence of densification on gauge factors α and γ is investigated comparing DPC model to perfectly plastic von Mises behavior with a yield strength of 7.5 GPa. For cohesive input a fracture energy $G = 0.0047$ GPa μm representing a fracture toughness of 0.825 MPa m$^{1/2}$. A maximum cohesive strength (MAXS) criterion was used for damage initiation followed by linear softening until final separation [37]. For indentation cracking

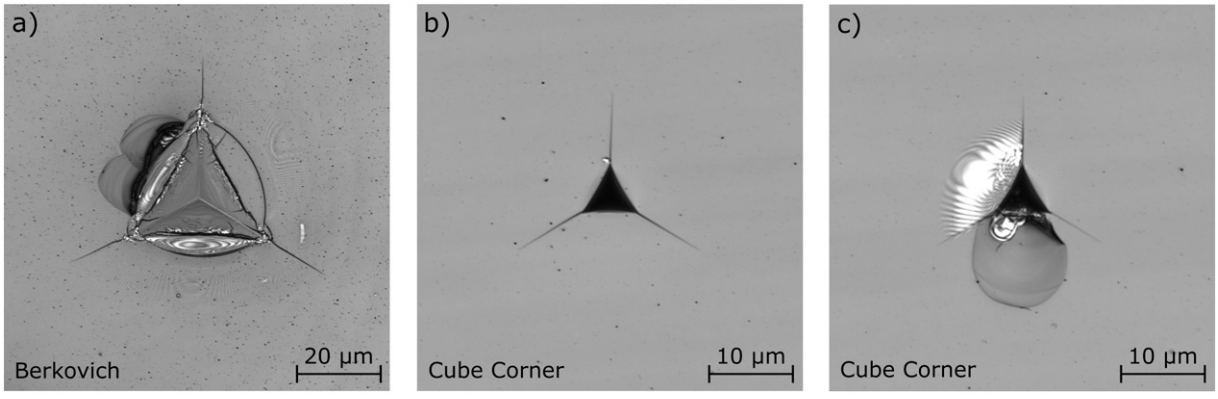

Fig. 3. Indentation cracking in fused silica. Multiple crack systems are activated by Berkovich indentation (a). Radial cracking dominates Cube Corner indentation (b) but is to about 90% accompanied by chipping (c).

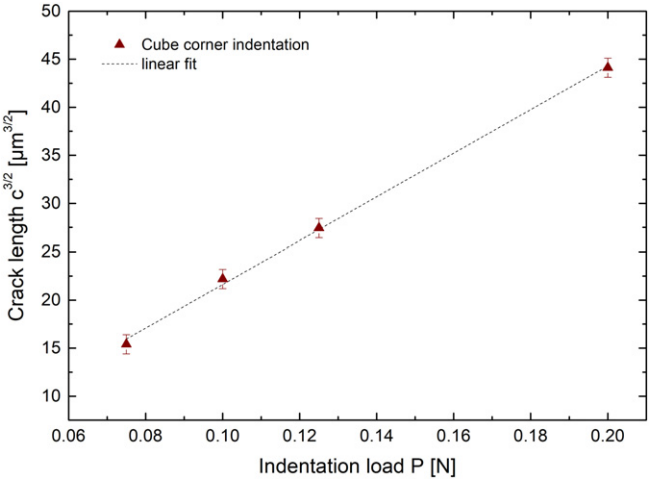

Fig. 4. Crack length $c^{3/2}$ as a function of the cube corner indentation load offers a linear relationship.

simulations a $\sigma_{max} = 0.3$ GPa was used as damage criterion, while pillar splitting simulations were found to require a larger σ_{max} of 0.5 GPa in order to minimize the process zone and to ensure that the load instability corresponds to the point when the crack reaches the pillars sidewall. An initial cohesive element stiffness or penalty stiffness of 1×10^4 (GPa) and a viscosity parameter of 1×10^{-6} (units of 1/time) were used in all simulations according to literature [38].

3. Results

3.1. Indentation cracking in fused silica

Indentation cracking in fused silica results in a mixed failure pattern if blunt indenter geometries such as Berkovich are used. Besides radial cracks, also cones, edge cracks and chipping can be observed (Fig. 3a). Fracture toughness determination according to LEM [16] cannot be performed, since energy dissipation is accompanied with all crack systems. Switching to the sharper cube corner indenter unifies the crack pattern and radial cracking becomes predominant (Fig. 3b). Indentation cracking with cube corner geometry was performed under ambient conditions for four loadings: 75, 100, 125 and 200 mN. In the present study in more than 90% of the indentations radial cracking was accompanied by chipping (Fig. 3c). Due to the reasons stated above only the remaining 10% which show pure radial cracking can be used for fracture toughness investigation according to Lawn, Evans and Marshall [16]. The crack length to the power of 3/2 plotted as a function of the indentation load (Fig. 4) exhibits a linear slope, thus confirming the LEM supposed relationship (Equation (1)).

3.2. Pillar splitting experiments on fused silica

Five different micro pillar geometries have been produced by DRIE. Conventional nanoindentation testing reveals a hardness $H = 9.56 \pm 0.09$ GPa and an elastic modulus $E = 72.1 \pm 0.4$ GPa for the used fused silica wafer. A second indentation matrix was performed in the etched region revealing DRIE not to influence E and H. Pillar splitting experiments were performed under ambient conditions on each of those geometries and an increasing splitting load has been observed with increasing micro pillar radius. The load displacement curves of the splitting experiments are exemplarily shown for the largest and smallest pillar geometry in Fig. 5a, whereas on average a larger splitting load is found for the largest pillar radius. A summary of the instability loads for all examined micro pillar geometries is provided in Fig. 5b and Table 1. The scatter is likely to be attributed to the positioning accuracy of G200 nanoindenter, equipped with an optical microscope.

Table 1
Summary of the instability load data for all examined micro pillar geometries.

Pillar radius r [µm]	Instability load $P_{Instability}$ [mN]			
	Max. value	Min. value	Average value	Standard deviation
3.27 ± 0.08	8.75	6.24	7.66	1.64
2.97 ± 0.07	7.73	5.36	6.56	0.87
2.69 ± 0.07	6.62	4.53	5.54	0.71
2.58 ± 0.06	6.33	4.61	5.63	1.81
2.34 ± 0.05	6.80	3.77	5.46	0.77

The pillar splitting experiments were repeated inside the SEM, which allows both a high positioning accuracy and the ability to observe the cracking process in-situ. While the former can easily be realized (Fig. 6a), the cracking process itself is under load control faster than the SEM scanning speed and can therefore not be recorded. Nevertheless, the fracture pattern provides helpful information on the pillar splitting behavior of fused silica. In most cases the pillar is completely vanished after testing. Fragments were rarely found, since DRIE pillar are free standing. In a few lucky cases fragments of former micro pillar can be found in the near vicinity of initial pillar location (Fig. 6b). Those fragments exhibit straight breaking edges along the longitudinal axis of the pillar height at an angle of roughly 120° to each other. This is illustrating that the micro pillar splitted into three parts, which perfectly matches the model assumptions [4,7] and validates the applicability of Equation (2) to estimate the fracture toughness from the load instability.

Pillar splitting experiments inside the SEM were found to reduce scatter but deliver instability loads significantly larger as those observed with the conventional nanoindenter under ambient conditions. For the smallest micro pillar radius for instance an almost three times larger load in the order of 13.4 mN was required for splitting the micro pillars. Even though it is known that an off-centered pillar splitting experiment leads to a reduced splitting load [31], it is unlikely that this huge offset can be attributed to the positioning accuracy alone since statistics should compensate this effect to some extent. Glass is known to be highly sensitive to atmospheric conditions [42] but also electron beam irradiation has been found to enhance its plasticity and fracture properties [2,35,43–46]. Indeed distinct differences can be observed comparing experiments where the e^- beam was turned on and turned off before starting the test (Fig. 7). When the e^- beam was turned off after positioning the splitting load decreases to about 9.7 mN accompanied with a significant reduction of scatter.

3.3. A FEA review of the gauge factors for fracture toughness estimation

An estimation of fracture toughness from indentation cracking and pillar splitting experiments according to Equations (1) and (2) require both knowledge of the corresponding gauge factors α and γ. In the present study FEA is used to review those gauge factors for the case of fused silica. The indentation process is modelled with both von Mises (pure shear flow) and Drucker-Prager-Cap plasticity (shear flow and densification) to investigate the densification effect on the gauge factors.

Crack propagation along the cohesive plane is visualized using the parameter SDEG [37], which indicates the stiffness degradation of a cohesive element ranging from 0 to 1, where a

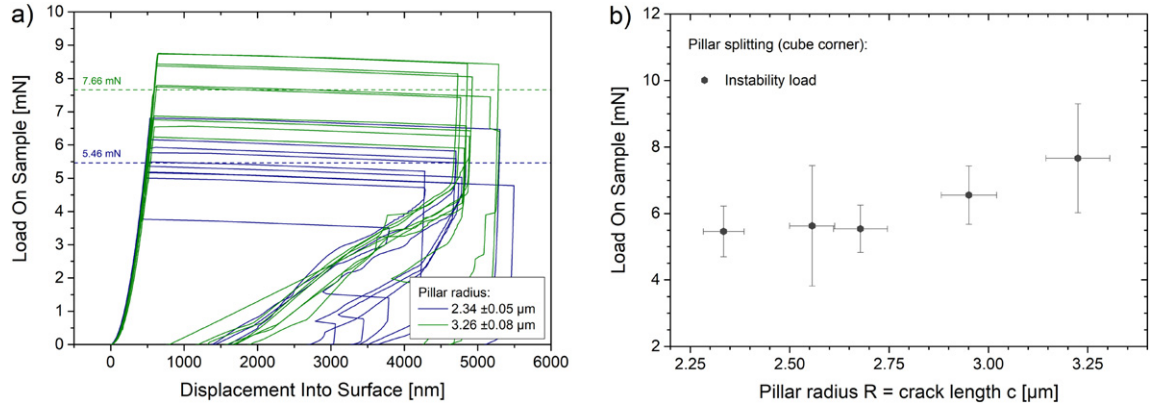

Fig. 5. a) Pillar splitting load displacement data exemplarily shown for the largest (green) and smallest (blue) pillar geometry. The average instability loads are sketched as dotted line and b) plotted with corresponding standard deviation as a function of the pillar radius. The corresponding values are summarized in Table 1.

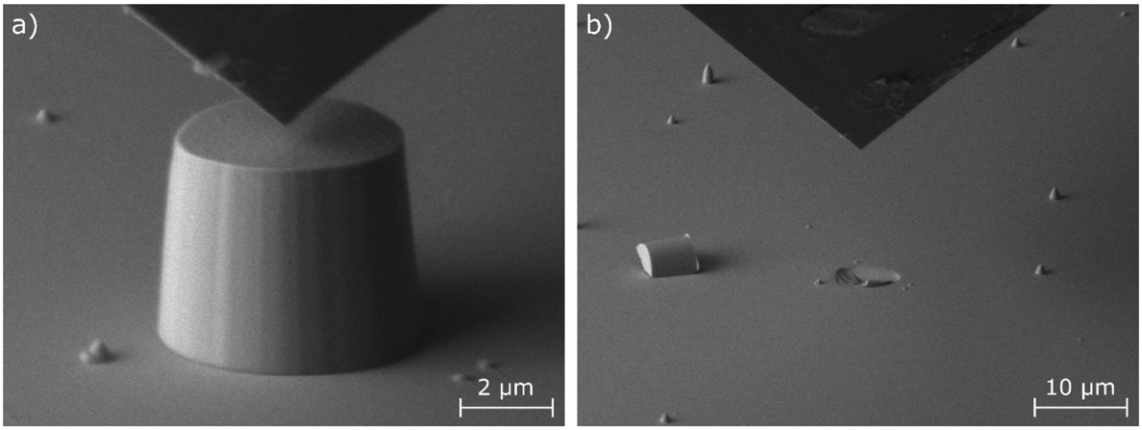

Fig. 6. Pillar Splitting inside SEM. a) The cube corner tip is carefully aligned in the center above the micro pillar. b) After splitting only a single fragment remained close to the previous pillar location.

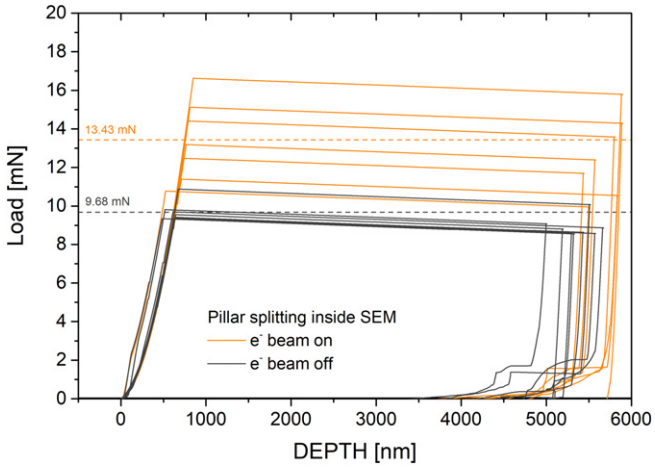

Fig. 7. Pillar splitting load displacement data recorded inSEM with both electron beam on and turned off while testing on micro pillar with a radius of 2.34 µm.

value of 1 represents full stiffness degradation or rather full element failure. The indentation cracking response with cube corner tip geometry delivers a roughly 8% smaller radial crack extension if densification is considered in the constitutive model. This corresponds well with observations made by Bruns et al. [11] on Berkovich geometry. The cracking sequence between Berkovich and cube corner geometry however differs significantly. With Berkovich geometry a subsurface median crack is forming during loading, expanding to a radial surface crack when compressive stresses in vicinity of the contact vanish upon unloading [11]. In turn, radial cracks develop with loading for cube corner geometry and their extension is interestingly unaffected by unloading (Fig. 8). This fundamental difference can be attributed to the plastic zone reaching the surface. Hence, it is less confined as with Berkovich indenter geometry. Tensile hoop stresses, responsible for crack opening [47], are present at the surface since beginning of loading. This is also the reason why the cube corners geometry harmonizes an indentation crack pattern (Fig. 3), whereas for blunter indenter geometries the variety of crack systems active upon unloading may demolish the residual impression and complicate fracture toughness treatments [15].

The continuous growing radial crack enables a quasi-continuous crack length determination during loading for certain indentation depths. According to Johanns et al. only crack lengths 10 times larger than the process zone size are considered, in order to reduce its influence within the calculation to below 5% [38]. The process zone for the given cohesive input can be estimated according to Dugdale to about 2.9 µm [11,38,48]. The linear relationship given in Fig. 9, where $c^{3/2}$ is plotted as function of the indentation load P, validates the applicability of Equation (1) and the gauge factor α is calculated from its slope. As densification slightly reduces the crack extension, von Mises plasticity exhibits a larger slope as the Drucker-Prager-Cap plasticity approach. As a consequence, gauge factors of $\alpha = 0.055 \pm 0.002$ and $\alpha = 0.052 \pm 0.002$ are determined for von Mises and DPC plasticity, respectively (Table 2). So the influence of densification is only slightly larger than the inherent uncertainty of α. It is worth noting that the error is of the order of magnitude that the consideration of a single additional cohesive element has on the α estimate. Those estimates are located at the upper end of the range for α (0.032–0.054) reported for cube corner geometry in literature [19–23]. Recent studies [18,25] renounce the general validity of α and emphasize it rather depends on the elastic plastic material properties such as E, H and ν. Therefore, the FEA estimate represents the material inherent alpha parameter for fused silica.

A similar investigation was performed for the pillar splitting approach. In contrast to the experimental setup (Fig. 5) the simulation is intrinsic displacement controlled. As a consequence, the pillar instability is accompanied with a load drop instead of a displacement jump (Fig. 10). Since densification enhances plasticity, the splitting event occurs at a slightly larger displacement using DPC plasticity. Interestingly this shift has almost no

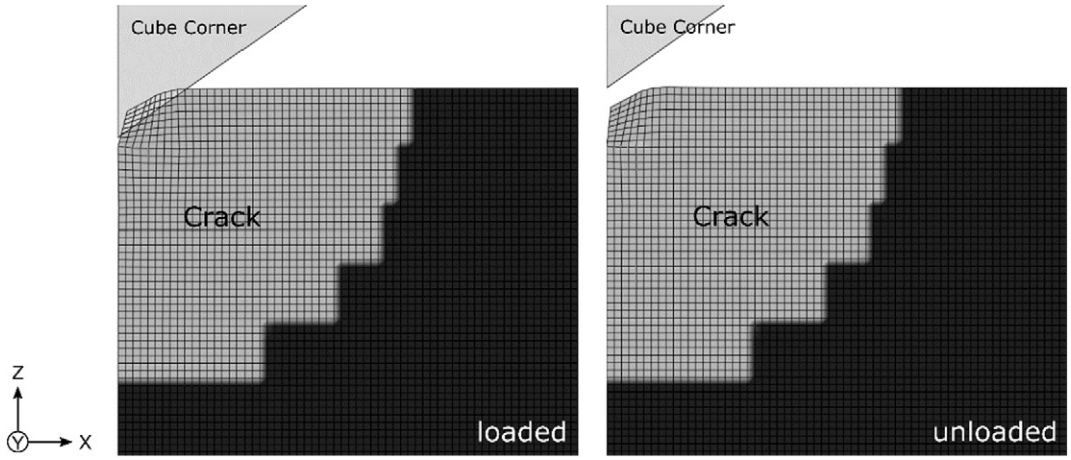

Fig. 8. Crack propagation along the cohesive plane in fused silica using cube corner tip geometry. The crack path (light grey) is visualized using the SDEG parameter while peak loading (left) and after unloading (right).

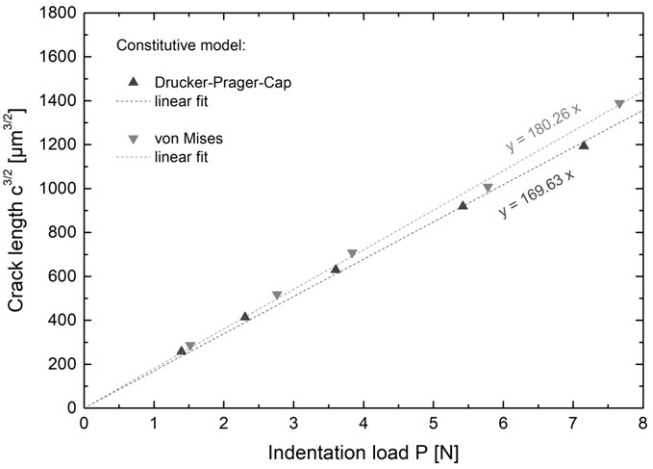

Fig. 9. Indentation cracking gauge factor α for cube corner tip geometry in fused silica. Densification reduces the crack length, hence slightly smaller α values can be determined with Drucker-Prager-Cap plasticity (dark grey).

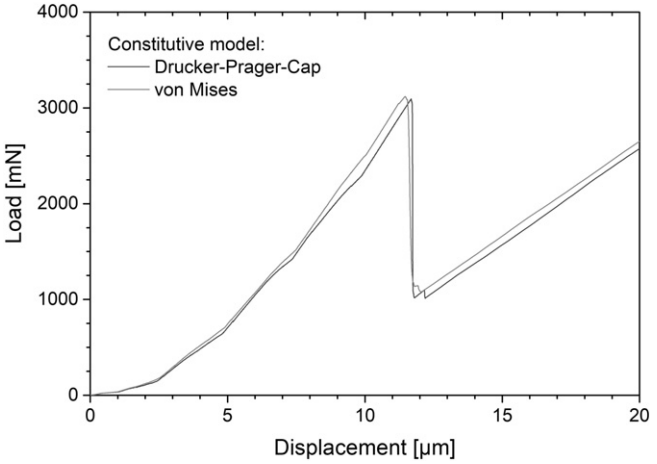

Fig. 10. Load displacement curve of a pillar splitting experiment from FEA. The colors indicate the different constitutive descriptions used as material input.

influence on the splitting load. In comparison to the experimental data, the splitting loads observed here are several orders of magnitude larger. This is due to a larger pillar size used in simulation to satisfy Johanns' rule of thumb that the crack lengths (pillar radius) has to exceed 10 times the process zone size [38]. The pillar splitting load can thereafter be used to calculate the gauge factor γ, since pillar dimensions and the cohesive input are known. In contrast to the indentation cracking simulations, each pillar splitting simulation allows for one γ estimate only. As a result $\gamma = 0.486$ and $\gamma = 0.490$ were determined for von Mises and Drucker-Prager-Cap plasticity, respectively (Table 2). The uncertainty of this estimate can be assessed introducing the size of a single cohesive element (which roughly corresponds to the process zone size) as uncertainty for the micro pillar radius R. This has an effect of ±0.007 on γ. The choice of constitutive model also affects Hardness, hence the E/H ratio. Plotting γ as function of E/H reveals that the slightly larger γ estimate using DPC plasticity could also be affected by the slightly larger E/H ratio (Fig. 11). In any case the effect of densification on γ is smaller than the inherent uncertainty in γ or the effect of E/H (if you compare to the linear slope of Ghidelli analysis [12]) and can be neglected for pillar splitting analysis. This corresponds well to investigations by Lacroix et al. [34] who found densification less pronounced in micro pillar compression experiments due to the vanished constraining effect of surrounding material.

For the given E/H ratio of roughly 7.5, a γ factor of 0.54 can be taken from the study of Ghidelli et al. [12] for the cube corner indenter geometry. The present study delivers a roughly 10% smaller value for γ. Pillar splitting simulations were found to be very sensitive to the choice of the cohesive input parameter, which most likely have caused this offset. Once the process zone in front of the crack becomes too large, the instability load does not correspond to the point when the crack is reaching the sidewall of the micro pillar anymore. The instability occurs earlier, therefore the process zone reduces the effective micro pillar radius and the γ estimate becomes larger. This effect was strongly pronounced using $\sigma_{max} = 0.3$ GPa as failure criterion in the present study. Increasing σ_{max} to 0.5 GPa was found to shift the instability event closer to the point when the crack is reaching the sidewall of the micro pillar. Therefore, this input parameter was assumed to deliver a more realistic description and thus more reliable γ values. Process zone effects in earlier studies [4,7,12] are, however, difficult to estimate.

3.4. Fracture toughness from indentation cracking techniques

The set of gauge factors delivered by cohesive zone finite element analysis allows to estimate the fracture toughness of fused silica from indentation crack lengths or pillar splitting loads. Calculating fracture toughness according to Equation (2) creates an almost constant values for both approaches if the scatter bars are considered (Fig. 12). The pillar splitting experiments are accompanied with larger scatter bars. The reason for this is mainly due to scatter in the splitting load, whereas the load is a controlled value in the indentation cracking approach and the error of K relies on scatter in the measured crack length only. In this manner average fracture toughness values of 0.68 and 0.67 MPa $m^{1/2}$ can be determined for indentation cracking and pillar splitting, respectively (Table 2). Those values are in good accordance with literature where a fracture toughness ranging from 0.58 to 0.78 MPa $m^{1/2}$ (sketched light grey in Fig. 12) is reported for fused silica [19,49–53]. Those results show that both techniques are capable to deliver reproducible fracture toughness data over a variety of pillar sizes and indentation loadings.

Inside the SEM, the changed atmospheric conditions and electron beam irradiation were found to increase the instability loads for pillar splitting (Fig. 7). This affects the fracture toughness estimate likewise (Fig. 13a). In fact, a fracture toughness of 1.85 MPa $m^{1/2}$ was determined if the electron beam was running while testing. But also in case the electron beam has been turned off before starting testing still an enhanced fracture toughness of about 1.25 MPa $m^{1/2}$ was observed. The ambient condition fracture toughness has therefore almost been tripled or doubled, respectively. This offset can clearly be attributed to e^- irradiation, which is known to activate (surface) atoms in silica glass. Bonds between Si–O pairs are broken and dangling bonds are formed [44]. In nanoscale silica e^- irradiation has been found to trigger superplastic deformation via an e^--beam assisted bond switching mechanism where dangling bonds recombine with neighboring defects to accommodate plastic flow [2,35,43,54]. Even though the micro pillars were about an order of magnitude larger it is conceivable that e^- irradiation has increased the bond energy in a surface layer [46]. Electron irradiation has even been found to enhance the fracture resistance of macroscopic fused silica where irradiation has been performed in an individual step before mechanical testing [45,46]. Consequently, e^- irradiation causes irreversible effects in glass. In this way, the positioning procedure (with e^- beam on) for the subsequent test with the e^- beam switched off before the start could also have had an influence, so that the enhanced splitting loads between inSEM and G200 can be attributed to this effect. Those results indicate that the inherent material properties should rather be tested under ambient conditions in a conventional nanoindenter.

Nanoindentation testing was performed under comparable conditions inside the SEM, too. Here no significant effect of electron beam irradiation on hardness and elastic modulus were noticed. This agrees well to the load displacement response of the micro pillars where the loading path is similar for pillar under and without irradiation (Fig. 7). The observed crack pattern, however, slightly differs if indentation is performed under electron beam irradiation. Fig. 13 (b and c) shows cube corner indentations loaded with 50 mN. A symmetric radial crack pattern as under ambient conditions (Fig. 3) is observed if the

Table 2
CZ FEA results for Indentation cracking and pillar splitting experiments.

Constitutive Model	H_{OP}[GPa]	E/H	α	γ
Von Mises	10.05	6.96	0.055 ± 0.002	0.486 ± 0.007
Drucker-Prager-Cap	9.60	7.29	0.052 ± 0.002	0.490 ± 0.007

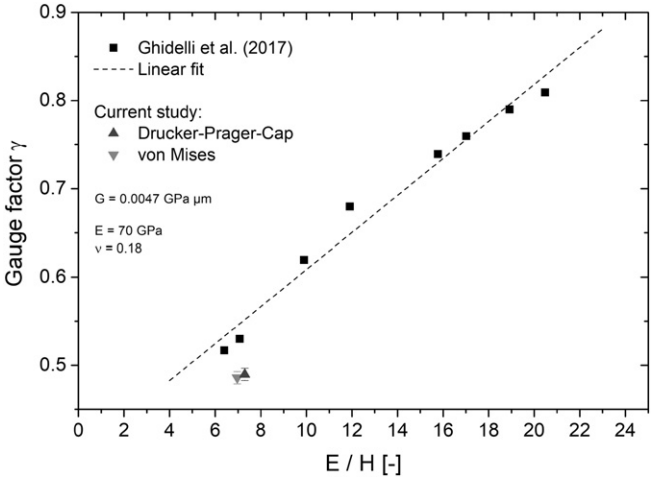

Fig. 11. Gauge factor γ for pillar splitting as a function of E/H ratio. The estimate for the cube corner indenter by Ghidelli et al. is plotted for comparison [12].

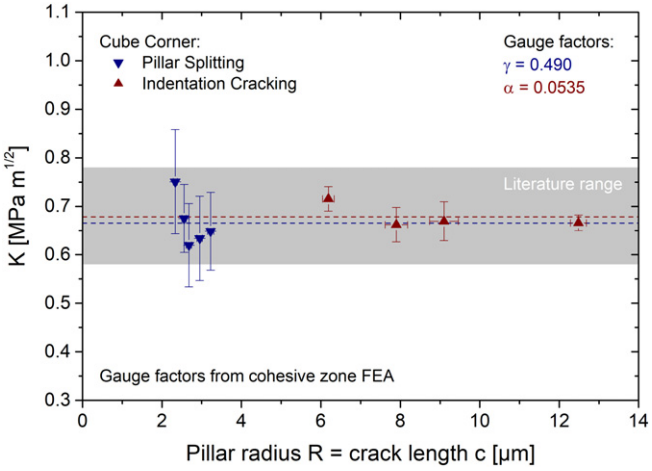

Fig. 12. Fracture toughness estimated using the gauge factors from cohesive zone FEA The fracture toughness range for fused silica reported in literature [19,49–53] is sketched light grey in the background.

electron been has been turned off before starting indentation testing (Fig. 13b). Under irradiation, however, the development of an asymmetric radial crack pattern can be noticed. The indenter edge pointing into the direction of the incident electron beam exhibits a roughly 30% smaller radial crack extension (Fig. 13c). A quantification of this effect is beyond the scope of the present study. However, there is an electron irradiation effect in conventional indentation cracking, too.

4. Conclusions

Indentation cracking and pillar splitting experiments were performed on fused silica in a conventional nanoindenter and inside a SEM using cube corner tip geometry. The micro pillars were fabricated using the lithography based deep reactive ion etching process. The whole study was accompanied by cohesive zone finite element simulations to review gauge factors under consideration of the anomalous deformation behavior of fused silica. It is found that both pillar splitting and cube corner indentation cracking yield similar fracture toughness values of about 0.68 MPa $m^{1/2}$ for pillar radii ranging from 2.3 µm to 3.3 µm and indent sizes from 1 µm to 5 µm depth. The measured fracture toughness thereby is close to values reported in literature. Therefore, pillar splitting as well as indentation cracking can be used to determine the fracture behavior of oxide glasses down to the µm regime. The detailed conclusions can be found in the following:

1. Pillar splitting experiments were found to be a promising alternative to conventional indentation cracking based methods when analysis becomes difficult due to simultaneously active crack systems. Especially for anomalous glasses, such as fused silica, rather a mixture crack systems than pure radial cracking is present. While cube corner indentation is capable to unify the crack pattern, radial cracking is largely accompanied by chipping which distorts a fracture toughness estimate. The results on pillar splitting experiments with cube corner tip geometry show that this technique can be applied for fused silica. The micro pillars are nicely splitted into three fragments (Fig. 6) according to the model assumptions [4,7] at loads too low to initiate chipping.
2. A review of the gauge factors for both indentation cracking based techniques using cohesive zone finite element modelling reveals significant differences from values present in literature, which confirms the non-existent general validity of α. Those shifts were found for both constitutive models used in the present study, thus they are not only an effect of densification.
3. The densification behavior of fused silica results in slightly smaller α values for indentation cracking; an offset only a little larger than the inherent uncertainty evoking from CZ FEA. For pillar splitting this effect is even smaller since the constraining effect of surrounding material is reduced and densification effects are lost in scatter and E/H effects. While the dependency of γ on E/H was already investigated in literature [12], there were still slightly smaller γ values found for fused silica in the present study. Pillar splitting simulations were found to be much more sensitive to the choice of the cohesive input parameter, which most likely has caused this offset. Therefore, both techniques, indentation cracking and pillar splitting, offer potential for further studies on the gauge factors for broader ranges of E/H ratios with optimized cohesive input parameters.
4. For fused silica the new set of gauge factors allows to determine similar fracture toughness values with both techniques, pillar splitting and indentation cracking (Fig. 12). This shows that the pillar splitting approach is a promising alternative to investigate fracture toughness of oxide glasses on the small scale.
5. Pillar splitting experiments inside the SEM have shown that electron irradiation is capable to enhance the fracture toughness of silica glass. As e^- irradiation is likely to occur in modern processing routes for micro and nano electromechanical devices, the altering effect of e^- irradiation is of prime importance for the components mechanical reliability. Even though this finding was only a side effect in the present study, it shows that micro pillar splitting experiments (and thus

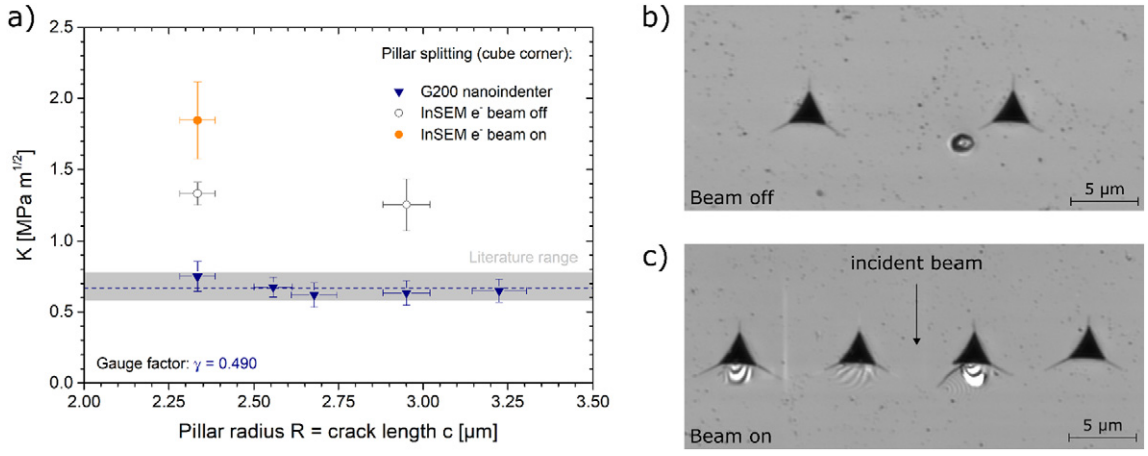

Fig. 13. a) Fracture toughness determined from pillar splitting experiments for various micro pillar geometries. Pillar splitting was performed under ambient conditions in a conventional G200 nanoindenter (blue) and inside the SEM with electron beam running (solid orange symbol) and electron beam turned off (open grey symbol) before testing. Bulk cube corner indentation performed inside SEM with b) electron beam turned off and c) turned on at same load of 50 mN. (For interpretation of the references to color in this figure legend, the reader is referred to the Web version of this article.)

probably also other micro scale geometries for fracture toughness evaluation; i.e. micro cantilever testing [4,5]) offer the potential to quantify fracture toughness not only after but also during e^- irradiation.

Data availability

The raw data required to reproduce these findings will be made available on request.

Conflicts of interest

The authors declare not conflict of interest.

CRediT authorship contribution statement

Sebastian Bruns: Conceptualization, Methodology, Investigation, Data curation, Formal analysis, Visualization, Writing - original draft. **Laszlo Petho:** Methodology, Writing - review & editing. **Christian Minnert:** Investigation, Writing - review & editing. **Johann Michler:** Methodology, Resources, Writing - review & editing. **Karsten Durst:** Conceptualization, Methodology, Writing - review & editing, Supervision, Project administration, Funding acquisition.

Acknowledgements

The authors gratefully acknowledge funding by the German Science Foundation (DFG) in priority program "SPP 1594 - Topological Engineering of Ultrastrong Glasses" and the Open Access Publishing Fund of Technische Universität Darmstadt.

References

[1] L. Wondraczek, J.C. Mauro, J. Eckert, U. Kühn, J. Horbach, J. Deubener, T. Rouxel, Towards Ultrastrong glasses, Adv. Mater. 23 (39) (2011) 4578–4586.
[2] K. Zheng, C. Wang, Y.Q. Cheng, Y. Yue, X. Han, Z. Zhang, Z. Shan, S.X. Mao, M. Ye, Y. Yin, E. Ma, Electron-beam-assisted superplastic shaping of nanoscale amorphous silica, Nat. Commun. 1 (2010) 24.
[3] T. Rouxel, S. Yoshida, The fracture toughness of inorganic glasses, J. Am. Ceram. Soc. 100 (10) (2017) 4374–4396.
[4] M. Sebastiani, K.E. Johanns, E.G. Herbert, G.M. Pharr, Measurement of fracture toughness by nanoindentation methods: recent advances and future challenges, Curr. Opin. Solid State Mater. Sci. 19 (2015) 324–333.
[5] J. Ast, M. Ghidelli, K. Durst, M. Göken, M. Sebastiani, A.M. Korsunsky, A review of experimental approaches to fracture toughness evaluation at the micro-scale, Mater. Des. 173 (2019) 107762.
[6] F. Iqbal, J. Ast, M. Göken, K. Durst, In situ micro-cantilever tests to study fracture properties of NiAl single crystals, Acta Mater. 60 (3) (2012) 1193–1200.
[7] M. Sebastiani, K.E. Johanns, E.G. Herbert, F. Carassiti, G.M. Pharr, A novel pillar indentation splitting test for measuring fracture toughness of thin ceramic coatings, Philos. Mag. 95 (16–18) (2014) 1928–1944.
[8] K.W. Peter, Densification and flow phenomena of glass in indentation experiments, J. Non-Cryst. Solids 5 (2) (1970) 103–115.
[9] F.M. Ernsberger, Role of densification in deformation of glasses under point loading, J. Am. Ceram. Soc. 51 (10) (1968) 545–547.
[10] A. Arora, D.B. Marshall, B.R. Lawn, Indentation deformation-fracture of normal and anomalous glasses, J. Non-Cryst. Solids 31 (3) (1979) 415–428.
[11] S. Bruns, K.E. Johanns, H.U.R. Rehman, G.M. Pharr, K. Durst, Constitutive modeling of indentation cracking in fused silica, J. Am. Ceram. Soc. 100 (5) (2017) 1928–1940.
[12] M. Ghidelli, M. Sebastiani, K.E. Johanns, G.M. Pharr, Effects of indenter angle on micro-scale fracture toughness measurement by pillar splitting, J. Am. Ceram. Soc. 100 (12) (2017) 5731–5738.
[13] T.M. Gross, J.J. Price, Vickers indentation cracking of ion-exchanged glasses: quasi-static vs. Dynamic contact, Front. Mater. 4 (2017).
[14] K. Januchta, M.M. Smedskjaer, Indentation deformation in oxide glasses: quantification, structural changes, and relation to cracking, J. Non-Cryst. Solids X (2019) 1.
[15] R.F. Cook, G.M. Pharr, Direct observation and analysis of indentation cracking in glasses and ceramics, J. Am. Ceram. Soc. 73 (4) (1990) 787–817.
[16] B.R. Lawn, A.G. Evans, D.B. Marshall, Elastic-plastic indentation damage in ceramics - the median-radial crack system, J. Am. Ceram. Soc. 63 (9–10) (1980) 574–581.
[17] G.R. Anstis, P. Chantikul, B.R. Lawn, D.B. Marshall, A critical-evaluation of indentation techniques for measuring fracture-toughness .1. Direct crack measurements, J. Am. Ceram. Soc. 64 (9) (1981) 533–538.
[18] J.H. Lee, Y.F. Gao, K.E. Johanns, G.M. Pharr, Cohesive interface simulations of indentation cracking as a fracture toughness measurement method for brittle materials, Acta Mater. 60 (15) (2012) 5448–5467.
[19] G.M. Pharr, Measurement of mechanical properties by ultra-low load indentation, Mater. Sci. Eng. A 253 (1–2) (1998) 151–159.
[20] G.M. Pharr, D.S. Harding, W.C. Oliver, Measurement of fracture toughness in thin films and small volumes using nanoindentation methods, in: M. Nastasi, D.M. Parkin, H. Gleiter (Eds.), Mechanical Properties and Deformation Behavior of Materials Having Ultra-Fine Microstructures, Springer Netherlands, Dordrecht 1993, pp. 449–461.
[21] D.S. Harding, W.C. Oliver, G.M. Pharr, Cracking during nanoindentation and its use in the measurement of fracture toughness, MRS Proceed. 356 (1994) 663.
[22] J.J. Chen, Indentation-based methods to assess fracture toughness for thin coatings, J. Phys. D Appl. Phys. 45 (20) (2012) 20300114pp.
[23] T.W. Scharf, H. Deng, J.A. Barnard, Mechanical and fracture toughness studies of amorphous SiC–N hard coatings using nanoindentation, J. Vac. Sci. Technol. A 15 (3) (1997) 963–967.
[24] K.E. Johanns, A Study of Indentation Cracking in Brittle Materials Using Cohesive Zone Finite Elements, University of Tennessee, 2014.
[25] H.C. Hyun, F. Rickhey, J.H. Lee, M. Kim, H. Lee, Evaluation of indentation fracture toughness for brittle materials based on the cohesive zone finite element method, Eng. Fract. Mech. 134 (2015) 304–316.
[26] J.-i. Jang, G.M. Pharr, Influence of indenter angle on cracking in Si and Ge during nanoindentation, Acta Mater. 56 (16) (2008) 4458–4469.
[27] D.J. Morris, S.B. Myers, R.F. Cook, Sharp probes of varying acuity: instrumented indentation and fracture behavior, J. Mater. Res. 19 (1) (2004) 165–175.
[28] B.A. Mound, G.M. Pharr, Nanoindentation of fused quartz at loads near the cracking threshold, Exp. Mech. 59 (3) (2019) 369–380.
[29] A.A. Volinsky, J.B. Vella, W.W. Gerberich, Fracture toughness, adhesion and mechanical properties of low-K dielectric thin films measured by nanoindentation, Thin Solid Films 429 (1–2) (2003) 201–210.
[30] K. Kese, D.J. Rowcliffe, Nanoindentation method for measuring residual stress in brittle materials, J. Am. Ceram. Soc. 86 (5) (2003) 811–816.
[31] C.M. Lauener, L. Petho, M. Chen, Y. Xiao, J. Michler, J.M. Wheeler, Fracture of Silicon: influence of rate, positioning accuracy, FIB machining, and elevated temperatures on toughness measured by pillar indentation splitting, Mater. Des. 142 (2018) 340–349.
[32] R. Ramachandramoorthy, J. Schwiedrzik, L. Petho, C. Guerra-Nunez, D. Frey, J.M. Breguet, J. Michler, Dynamic plasticity and failure of microscale glass: rate-dependent ductile-brittle-ductile transition, Nano Lett. 19 (4) (2019) 2350–2359.
[33] R. Lacroix, V. Chomienne, G. Kermouche, J. Teisseire, E. Barthel, S. Queste, Micropillar testing of amorphous silica, Int. J. Appl. Glass Sci. 3 (1) (2012) 36–43.
[34] R. Lacroix, G. Kermouche, J. Teisseire, E. Barthel, Plastic deformation and residual stresses in amorphous silica pillars under uniaxial loading, Acta Mater. 60 (15) (2012) 5555–5566.
[35] M. Mačković, T. Przybilla, C. Dieker, P. Herre, S. Romeis, H. Stara, N. Schrenker, W. Peukert, E. Spiecker, A novel approach for preparation and in situ tensile testing of silica glass membranes in the transmission electron microscope, Front. Mater. 4 (2017).
[36] W.C. Oliver, G.M. Pharr, An improved technique for determining hardness and elastic-modulus using load and displacement sensing indentation experiments, J. Mater. Res. 7 (6) (1992) 1564–1583.
[37] *Abaqus 2016 Online Documentation*: Dassault Systèmes2015.
[38] K.E. Johanns, J.H. Lee, Y.F. Gao, G.M. Pharr, An evaluation of the advantages and limitations in simulating indentation cracking with cohesive zone finite elements, Model. Simul. Mater. Sci. Eng. 22 (1) (2014), 015011.
[40] G. Kermouche, E. Barthel, D. Vandembroucq, P. Dubujet, Mechanical modelling of indentation-induced densification in amorphous silica, Acta Mater. 56 (13) (2008) 3222–3228.
[41] O. Benzine, S. Bruns, Z. Pan, K. Durst, L. Wondraczek, Local deformation of glasses is mediated by rigidity fluctuation on nanometer scale, Adv. Sci. 5 (10) (2018) 1800916.
[42] T.K. Bechgaard, J.C. Mauro, M.M. Smedskjaer, Time and humidity dependence of indentation cracking in aluminosilicate glasses, J. Non-Cryst. Solids 491 (2018) 64–70.
[43] M. Mačković, F. Niekiel, L. Wondraczek, E. Bitzek, E. Spiecker, In situ mechanical quenching of nanoscale silica spheres in the transmission electron microscope, Scr. Mater. 121 (2016) 70–74.
[44] D.L. Griscom, E.J. Friebele, Effects of ionizing radiation on amorphous insulators, Radiat. Eff. 65 (1–4) (1982) 63–72.
[45] K. Iwata, Y. Nishi, Effect of electron-beam irradiation on impact value of silica glass, Mater. Trans. 49 (9) (2008) 2058–2062.
[46] Y. Nishi, A. Kadowaki, T. Sinoda, Influence of electron beam irradiation on bending fracture stress for soda glass, Mater. Trans. 45 (12) (2004) 3314–3317.
[47] B. Lawn, R. Wilshaw, Indentation fracture: principles and applications, J. Mater. Sci. 10 (6) (1975) 1049–1081.
[48] T.L. Anderson, Fracture Mechanics: Fundamentals and Applications, third ed. Taylor & Francis, Boca Raton, 2005.
[49] J.P. Lucas, N.R. Moody, S.L. Robinson, J. Hanrock, R.Q. Hwang, Determining fracture toughness of vitreous silica glass, Scr. Metall. Mater. 32 (5) (1995) 743–748.
[50] G. Žagar, V. Pejchal, M.G. Mueller, L. Michelet, A. Mortensen, Fracture toughness measurement in fused quartz using triangular chevron-notched micro-cantilevers, Scr. Mater. 112 (2016) 132–135.
[51] M.G. Mueller, V. Pejchal, G. Žagar, A. Singh, M. Cantoni, A. Mortensen, Fracture toughness testing of nanocrystalline alumina and fused quartz using chevron-notched microbeams, Acta Mater. 86 (2015) 385–395.
[52] J.A. Salem, V. Sglavo, Transparent armor ceramics as spacecraft windows, J. Am. Ceram. Soc. 96 (1) (2013) 281–289.
[53] S. Wiederhorn, H. Johnson, A. Diness, A. Heuer, Fracture of glass in vacuum, J. Am. Ceram. Soc. 57 (8) (1974) 336–341.
[54] K.-i. Nomura, Y.-C. Chen, R.K. Kalia, A. Nakano, P. Vashishta, Defect migration and recombination in nanoindentation of silica glass, Appl. Phys. Lett. 99 (11) (2011) 111906.